Journal of Photochemistry & Photobiology, A: Chemistry 457 (2024) 115884

Contents lists available at ScienceDirect

Journal of Photochemistry & Photobiology, A: Chemistry

journal homepage: www.elsevier.com/locate/jphotochem

Advanced one pot photochemical surface modification approach towards graphene materials and their application in dye removal

Aminu Magaji [a,b], David P. Martin [b], Li-Shang Lin [c], Sergey A. Krasnikov [d], Alexander Kulak [b], Zabeada Aslam [c], Rik Drummond-Brydson [c], Natalia N. Sergeeva [a,d,*]

[a] School of Design, University of Leeds, Leeds LS2 9JT, UK
[b] School of Chemistry, University of Leeds, Woodhouse Lane, Leeds LS2 9JT, UK
[c] School of Chemical and Process Engineering, University of Leeds, UK
[d] The Leeds Institute of Textiles and Colour, University of Leeds, Leeds LS2 9JT, UK

ARTICLE INFO

Keywords:
Photochemistry
Graphene
Diazonium surface modification
TEM
Adsorption
Dye removal
Environmental remediation

ABSTRACT

Carbonaceous materials have shown undisputable promise as adsorbents and catalysts in various applications. The ability to tune key features such as specific surface area and functionality to improve the activity, represents a key advantage. However, this requires the development of general and versatile synthetic methods to deliver these multifunctional materials. This work reports a convenient general approach to prepare a series of graphene-chromophore systems. Two photochemical methods involving a step-by-step procedure and a one-pot method were compared. It was found that the two-step procedure is limited by the stability of the diazonium salts and thus has a limited application. The one-pot method allows preparation of a wide range of different composites in an easy and inexpensive manner. Synthesised samples were characterised by a range of methods including electron microscopy, X-ray diffraction, infra-red spectroscopy and gas adsorption. Transmission electron microscopy analysis revealed an ordered array of chromophores on the surface of the graphene nanoplatelets. The samples were tested as potential materials for dye removal; these studies revealed that most graphene-chromophore materials can successfully remove organic pollutants such as methylene blue, rhodamine B and methyl orange from aqueous media.

1. Introduction

Environmental pollution with organic compounds, known as emerging contaminants, is one of leading causes for concern as conventional water treatment plants do not remove these contaminants efficiently [1]. Adsorption remains a promising process to remove these pollutants since it provides low initial costs, a simple design and a choice of adsorbents [1,2]. Moreover, the combination of adsorption and catalytic oxidation by carbonaceous materials such as biochar [3,4], reduced graphene oxide [5], carbon nanotubes [6], g-C_3N_4 [7] have emerged as potential alternatives [2,8]. Their ability to remove pollutants through (non–) radical pathways [3] is driven by the availability of reactive groups. Graphene is well suited to remove emerging contaminants, which are present at low concentrations and generate a hazard to the environment [9]. Graphene also has distinct advantages over composites of transition metals because it is relatively inexpensive, environmentally friendly, non-toxic and produces no secondary pollution [10]. However, it is highly hydrophobic and has a tendency to aggregate. Moreover, a lack of functionalities limits graphene's adsorption capability to pi-pi interactions, and irreversible trapping of pollutants is difficult to achieve. Although graphene-based materials have emerged as highly promising candidates for a variety of applications [11–17] including strong potential in processes such as photoreduction of CO_2 [18], Fischer-Tropsch synthesis [19], water splitting [20–22], and water treatment [23–25], the materials involved in these transformations normally contain metal-based active centres [26,27], whereby graphene simply plays the role of a support material. This is partially due to pristine graphene having a low density of (electronic) states (DOS) near

Abbreviations: Acr, Acridine; An-OH, 2-Hydroxy Anthroquinone; Chr, Chromone; FFT, Fast Fourier Transformation; Fsc, Fluorescein; FTIR, Fourier Transform Infrared Spectroscopy; GP, Graphene Nanoplatelets; MB, Methylene Blue Dye; Pnz, Phenazine; SEM, Scanning Electron Microscopy; TEM, Transmission Electron Microscopy; Thio, Thionine; UV/vis, Ultraviolet/Visible; XRD, powder X-Ray Diffraction.

* Corresponding author at: School of Design, University of Leeds and The Leeds Institute of Textiles and Colour, University of Leeds, Leeds LS2 9JT, UK.
E-mail address: n.sergeeva@leeds.ac.uk (N.N. Sergeeva).

https://doi.org/10.1016/j.jphotochem.2024.115884
Received 17 April 2024; Received in revised form 22 June 2024; Accepted 8 July 2024
Available online 9 July 2024

the Fermi level, and therefore, the activity is driven by the intrinsic characteristics of the non-graphene component of the system [28–30]. Consequently, in order to create truly metal-free systems based on graphene this requires the manipulation of electronic properties through the tuning of its band structure [31–34]. This can be readily achieved by functionalisation of the graphene basal plane *via* chemisorption, physisorption or doping with heteroatoms [10,35–37]. These approaches can be used to create defects and active sites on the graphene surface [10,36,37], significantly expanding its potential as a (photo)catalyst. Moreover, its dispersibility in common organic solvents and water can also be improved through a lowering of the surface energy [10]. Covalent functionalisation is a more suitable pathway to fabricate materials for environmental remediation, because it leads to more prominent changes in the electronic properties due to the disruption of the crystal lattice [38,39], this in turn helps to create active sites for catalysis and efficient adsorption. Thus, significant efforts aimed at covalent functionalisation of the graphene surface in order to tune the band gap and modulate its doping level have been undertaken [40]. Due to the inert nature of the sp^2-hybridised lattice of the pristine graphene basal plane, covalent modification involves reaction with reactive radicals or dienophiles [36,37,41].

We have previously reported a two-step photochemical method using radical grafting induced by white light to produce a graphene-phenazine hybrid with improved solubility and a modified band gap [42]. Here, we report, for the first time, a general photochemical methodology that can be applied to a wide range of structurally different molecules to fabricate a diverse family of graphene-chromophore systems in an easy and cost-effective manner. We have also evaluated their ability as new materials for dye removal using a combined adsorption and photocatalytic strategy.

2. Experimental section

2.1. Materials and methods

Graphene nanoplatelets (GP) were obtained from Sigma-Aldrich. All reagents were obtained from Sigma-Aldrich and Acros Organics and used as received. All reactions were stirred with a magnetic stirrer unless otherwise stated. Infrared spectra (IR) were recorded from the solid phases using a Bruker Alpha Platinum ATR FTIR spectrometer. The electronic absorption spectra were recorded using a Cary 100 UV–Vis scanning spectrophotometer. Spectrophotometric experiments to assess the photocatalytic and adsorption abilities of the materials were carried out using a Cary 50 UV–Vis spectrophotometer controlled at 20 °C by a single cell Peltier accessory, while Mercury and Xenon lamps were employed as the source of visible and UV lights, respectively. Thermogravimetric analysis (TGA) of the samples was undertaken on an SDT-Q600 Simultaneous TGA with heating rate 5 °C per minute. X-Ray diffraction (XRD) of the materials were recorded on Bruker D2-Phaser diffractometer using Cu Kα radiation, with a step size of θ = 0.01013°; Lorentzian fitting was used to measure the full width at half maxima (FWHM) of the diffraction peaks. Brunauer-Emmett-Teller (BET) surface area measurements were performed using a Micromeritics TriStar 3000 instrument; samples were degassed in N_2 at 110 °C for 3 h before analysis and N_2 adsorption and desorption isotherms were measured at 77 K. Transmission electron microscopy (TEM) analysis was carried out using the FEI Titan Themis Cubed operated at 80 kV; samples were prepared by dispersing the powders in IPA, sonicating and then drop casting onto holey carbon TEM grids and bright field TEM images were collected on a Gatan Oneview 16Megapixel CMOS detector.

2.2. General procedure to fabricate graphene-dye systems

Amino compounds used to generate diazonium salts are 7-amino-2-methylchromone, 9-aminoacridine, 2-amino-3-methyl-8-dimethylaminophenazine (Neutral Red), thionine, 4′-aminofluorescein.

Method A [42]. In brief, an appropriate amino compound (5.04 mmol) was dissolved in HBF_4 (7 mL; 50 % w/w H_2O) and stirred. Then, sodium nitrite (5.04 mmol, 0.35 g) in 2 mL of H_2O was added dropwise and the reaction was left stirring for 2 h. A small volume of diethyl ether (5 mL) was added and the diazonium salt was collected by vacuum filtration. Graphene (50 mg) was suspended in EtOH (100 mL) and sonicated for 30 min. A solution of the diazonium salt (0.262 mmol) was added to the graphene suspension, and the mixture was illuminated with white LED light (2,000 lm) for 2 h under stirring. The resulting dark coloured solution was washed several times with distilled water and ethanol, centrifuged at 6000 rpm until no colour was observed in the supernatant. The materials were dried and collected as black powders.

Method B. Typically, 80 mg of an appropriate amino compound was dissolved in 100 mL of ethanol in a 250 mL conical flask. 8 mL of 50 % HBF_4 was added to the solution, followed by 40 mg of $NaNO_2$ at 0 °C and stirred for 40 min to generate the diazonium salt. 100 mg of graphene nanoplatelets suspended in EtOH were added to the *in situ* generated diazonium salt. The resulting mixture was illuminated with white light (LED > 2,000 lm) for two hours under stirring. The resultant dark coloured solution was washed several times with distilled water and ethanol and centrifuged at 6000 rpm until no colour was observed in the supernatant. The materials were dried and collected as black powders.

2.3. Adsorption studies for dye removal using spectrophotometric analysis

Optimal loading studies and standardisation curves for methyl orange (MO), methylene blue (MB) and rhodamine B (RhB). All adsorption studies were carried out without illumination. The extinction coefficients of the dyes (adsorbates) were determined experimentally (See Supporting Information Sec. 3) and were as follows: 0.2599 L(mg cm)$^{-1}$ (MB), 0.1025 L(mg cm)$^{-1}$ (MO) and 0.2622 L(mg cm)$^{-1}$ (RhB). In all experiments the light path length was 1 cm. The mass loading experiments were carried out using the following range of concentrations for graphene materials in g/L: 0.0164, 0.0244, 0.0323, 0.04, 0.0476, 0.0551 and 0.0625. The procedure follows one described in the section below '*The kinetics study of dye removal*', where optimal loading (0.0323 g/L) is replaced by relevant concentration of GP-material. The study is done for one cycle of dye removal.

Adsorption capacity (q_t) or loading of adsorbate (dye) on the adsorbent (surface) was calculated as follows: $q(t) = (C_0 - C_t)/C_s$, *where C_0 is the initial adsorbate concentration (mg per L), C_t is the dye concentration in the solution at any given time (t) (mg per L), and C_s* is the concentration of adsorbent (*g per L*). Using the Lambert-Beer Law: $q(t) = (A_0 - A_t)/(\varepsilon|C_s)$, where A_0 and A_t are absorbances of the dye in the cuvette at t = 0 and n min, respectively; ε is extinction coefficient of the dye and l is the pathlength (1 cm). (SI Table S3).

The kinetics study of dye removal. 0.03 mL of a dye stock solution of MB, RhB or MO was added into a quartz cuvette containing 3 mL of distilled water to ensure that optical transmission falls within acceptable range (Abs 0.7–1.0 a.u.) prior adding graphene materials. The solution was stirred to achieve homogeneity, and a UV–vis absorption spectrum was recorded and used as 0 min value (A_0). To the quartz cuvettes containing 0.0323 g/L of the appropriate GP-material (0.1 mL of the stock sol. 1 mg/mL) in 3 mL of water, 0.03 mL of MB stock solution was added and stirred for 1 min prior the first scan. A kinetics experiment was carried out for 120 min, by recording UV–vis spectra at 1 min, 20 min, 40 min, 60 min, 80 min, 100 min and 120 min. Dye removal efficiency was determined by plotting a graph of At/Ao against time (minute) using the formula: $\%\text{Dye Removal} = [(A_0\text{-}A_t)/A_0] \times 100\ \%$; where A_0 and A_t are the absorbances at 664 nm at $t_0 = 0$ min, and at various time points t = 1 min, 20 min, 40 min, 60 min, 80 min, 100 min and 120 min. The experiments were performed in triplicate and the mean values are reported.

The non-linear fitting was carried out in OriginPro using the following equations:

$$\text{Pseudo}-\text{first}-\text{order (PFO)}: qt = qe^{*}(1 - e^{k1^{*}t}) \quad (1)$$

$$\text{Pseudo}-\text{second}-\text{order (PSO)}: qt = (qe^{2}{*}k2{*}t)/(1 + qt{*}k2{*}t) \quad (2)$$

3. Results and discussion

3.1. Materials fabrication

We have previously reported a method for graphene modification with phenazine dye, which can be carried out on both quasi free-standing (graphene/SiC(0 0 1)) [43] and multi-layer graphene (nanoplatelets, ca. 10 layers) [42]. This method (Fig. 1 Method A) is a two-step process and relies on the production of diazonium salt from the corresponding amine of the organic compound. Firstly, a stable diazonium salt is generated and isolated followed by a second step, which involves the photochemical reaction between graphene and the diazonium salt. However, this approach requires prior preparation and isolation of the diazonium salt which may exhibit instability greatly limiting the applicability of the method. Moreover, the tedious process of purification of the diazonium salt prior to the second step limits its overall efficiency.

To overcome these issues, we have developed an alternative synthetic methodology (Fig. 1 Method B), which can be applied to a variety of different amines and requires no prior isolation of the corresponding diazonium salts. In Method B, the fabrication of graphene-chromophore system is carried out as a one-pot procedure. Here, the diazonium salt is generated *in situ* avoiding unnecessary isolation by stirring $NaNO_2$ and the corresponding amine for 40 min at low temperature. Then, graphene nanoplatelets are added directly to the mixture; and illumination with white light initiates the reaction between graphene and the diazonium salt. Here, we demonstrate that this method provides access to a series of graphene-chromophore systems containing chromone (**GP-Chr**), acridine (**GP-Acr**), phenazine (**GP-Pnz**), fluorescein (**GP-Fsc**), 2-hydroxy anthraquinone (**GP-AnOH**) and thionine (**GP-Thio**).

Importantly, both methods require illumination with white light for modification of the graphene surface, including those chromophores which have no absorption in the visible region. This observation further confirms our suggestion that hot electrons in graphene are responsible for the initial step of electron transfer from the occupied states of graphene to unoccupied states of diazonium salt, releasing nitrogen gas and generating a chromophore based radical.

3.2. Materials characterisation

Successful modification of the graphene nanoplatelets was verified by FT-IR, XRD, BET and UV–vis analysis. In Fig. 2**a**, FTIR spectra for the series shown between 1900 and 750 cm^{-1}, are notably different from unmodified GP as the GP spectrum is almost featureless. All materials have enhanced and new bands between 1900 and 1500 cm^{-1} region corresponding to C = C, C = O (conjugated), C = N stretches. The fingerprint region (1500–750 cm^{-1}) shows a range of C-O (aromatic) and C–N (aromatic) stretches, N-H and O-H bending modes and a range of C = C and =C–H bending modes (out-of-plane), as well as the ring torsion bending vibrations.

Optical properties of the modified graphene samples were substantially altered compared to unmodified GP, which shows a typical absorption band at 270 nm. UV–vis spectra of the materials shown in Fig. 2**b**, demonstrate that the modified materials containing a visible light absorbing chromophore have additional bands in the visible region e.g. GP-Pnz (λ_{vis} 461 nm), GP-Acr (λ_{vis} 403 nm, 428 nm), GP-Fsc (λ_{vis} 455 nm, 488 nm), GP-Thio (λ_{vis} 601 nm, 652 nm), which matches the optical behaviour of the chromophore itself. Also, GP-Chr and GP-AnOH demonstrate significant broadening of the UV-band between 300 and 400 nm due to efficient π-π* transitions in these chromophores, which are strong UV-absorbers. In addition, the UV spectrum of GP-AnOH tails off into visible region, although no well-resolved bands can be observed.

3.2.1. Thermogravimetric analysis (TGA)

Thermogravimetric analysis (TGA) was carried out for unmodified GP, the GP-functionalised samples and the starting amines between 50 and 900 °C (Fig. S1, in SI) and Fig. 2**c,d** show normalised first derivatives (DTGA). For all graphene samples, the initial mass loss due to moisture and adsorbed air is observed below < 50 °C. A complete pyrolysis of unmodified graphene is achieved by 710 °C, which corresponds to 99.4 % of the total mass loss which can be used as a purity check. The starting dyes have two key degradation regions between 170–370 °C and 370–620 °C, while the pyrolysis of the functionalised materials occurs within 570–820 °C range. The total %mass loss and the inflection temperatures (T_i) are summarised in Table 1. The total mass loss varies between 97.5 % and 100 % indicating a high purity of the materials in terms of their graphitic content. After the initial loss of moisture and adsorbed air, DTGA of unmodified graphene shows only one significant region with the inflection temperature of 637 °C.

Initial amines of chromone, acridine and anthraquinone show a fast thermal degradation process between 269–315 °C followed by a slower

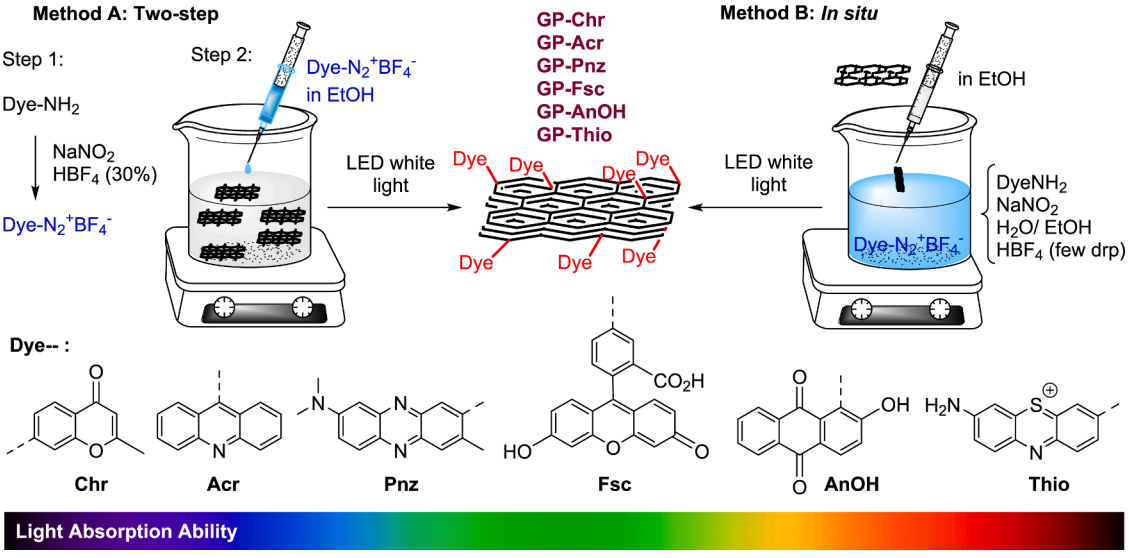

Fig. 1. General strategies for fabricating graphene-dye composites: Method A (two-step procedure) and Method B (*in situ* one-pot).

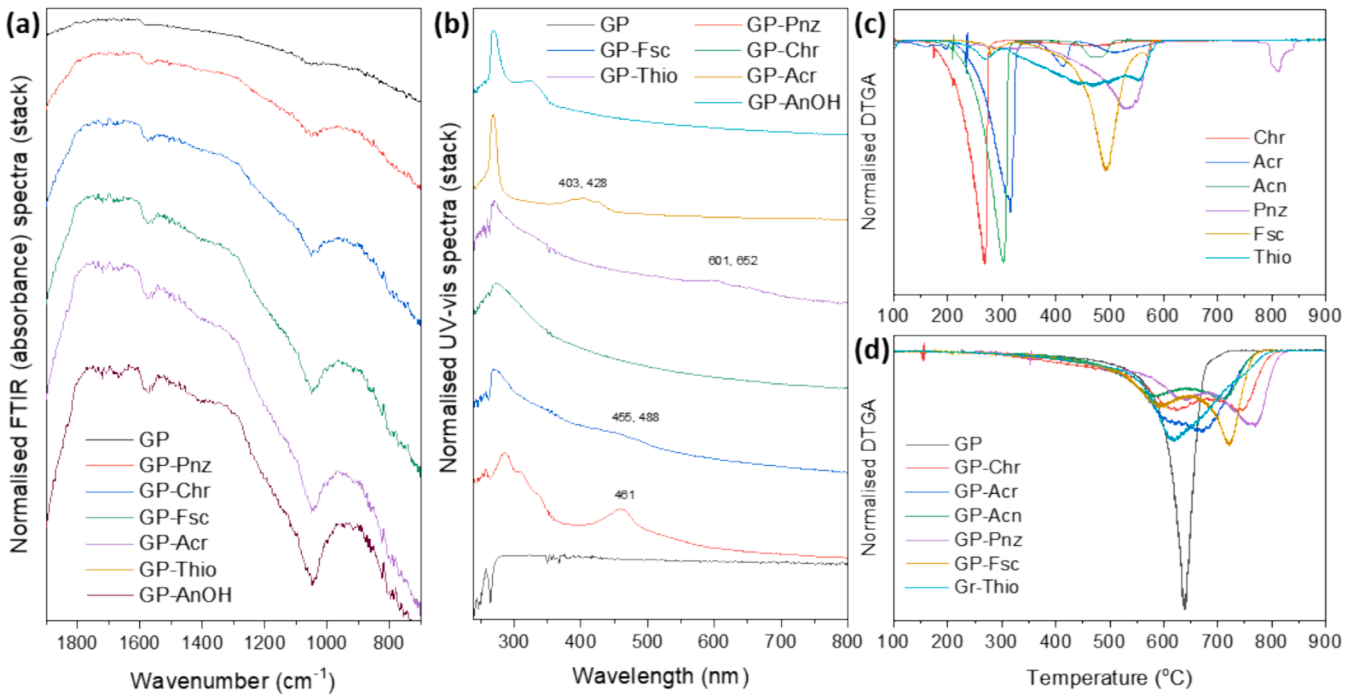

Fig. 2. (a) Normalised FTIR spectra (absorbance mode) of the materials; (b) Normalised UV–vis absorption spectra of the materials in water. TGA first derivative (DTGA) plots for (c) starting amines and (d) graphene and modified graphene samples.

Table 1
Total %mass loss and the inflection temperatures of (T_i) for the graphene composites and their corresponding starting dyes. (f = fast; s = slow process).

GP-sample	T_i, °C	Total mass loss, %	Starting amine	T_i, °C	Total mass loss, %
graphene	637	99.4	–	–	–
GP-Chr	620, 744	99.4	Chr	269f, 462 s	92.3
GP-Acr	613, 670	100	Acr	315f, 413 s, 508 s	99.8
GP-Acn	590, 710	97.5	Acn	304f, 475 s	100
GP-Pnz	632, 764	97.6	Pnz	302 s, 533f, 809 s	97.3
GP-Fsc	595,721	99.7	Fsc	278 s, 493f	98.8
GP-Thio	620f, 737 s	97.8	Thio	268 s, 456f, 555 s	100

process at a higher temperature (462–508 °C), while the fast process for phenazine, fluorescein and thionine, occurs at a higher temperature range (493–555 °C).

The inflection temperatures attained from DTG analysis show distinct differences between starting materials and the modified graphene samples. The degradation pattern of the modified graphene samples prepared by radical method shows two key regions with inflection temperatures ranges of 590–632 °C and 670–764 °C, respectively. These regions can be attributed two types of material: graphene with sp^3 defects due to radical reaction on the outer nanoplatelets' sheets and non-modified graphene of higher crystallinity with preserved sp^2 hybridisation across basal plane (inner nanoplatelets' sheets). Both ranges show a comparable rate suggesting that the first range with the lowest (T_i) is likely due to the degradation of the defected graphene (due to the functionalisation). While the second stage with a higher temperature of graphene pyrolysis can be explained by the thermal degradation of aggregated graphene nanoplatelets which thermal stability is similar to graphite.

3.2.2. XRD and BET analysis

XRD patterns were recorded for non-modified and modified samples showing diffraction peaks at 26.6 (002), 44.6 (101) and 54.7 (004), which are typical for graphene nanoplatelets. Lorentzian peak fitting of the (002) peak provided FWHM (°) and d_{002} (Å) data which are summarized in Table 2 and **SI Fig. S2**. No significant changes to the structure of the nano flakes were observed upon modification; the FWHM values for the modified samples increased by 12–38 % as compared to the unmodified GPs. This could be attributed to strain induced by the modification, which can also lead to the reduction of graphene sheets in individual nanoflakes. The d_{002}-spacings do not show any significant variation from the unmodified sample; this indicates that no residual chemical species is present in the interlayer space as d_{002} = 3.32–3.33 Å is too small to contain entities as large as an epoxy group (1.25 Å) or a water molecule (2.75 Å) [44]. This confirms that the chemical signatures observed in IR spectra are on the surface of the GP.

BET analysis revealed a stark reduction in the specific surface area (SSA) of the modified GP samples as compared to original GP (430 m^2/g). The data summarised in Table 2, shows that the surface area was reduced by 65 % for GP-Pnz closely followed by GP-Chr, GP-Thio and GP-AnOH, when compared to unmodified GP. The apparent SSA reduction along with TGA results indicates modification of the graphene surface by chromophore moieties. Although, some of the change in SSA could be attributed to an increased aggregation of the modified platelets (compared to pure GP) partially restricting nitrogen access to the GP

Table 2
Summary of XRD data of the (002) peak and BET data for GP and the modified samples.

	2θ (°)	FWHM, (°)	d_{002}, (Å)	SSA, (m^2/g)
GP	26.77	0.615	3.33	430
GP-Chr	26.79	0.730	3.33	201
GP-Acr	26.78	0.745	3.33	301
GP-Pnz	26.75	0.694	3.33	152
GP-Fsc	26.78	0.729	3.33	271
GP-AnOH	26.79	0.790	3.33	246
GP-Thio	26.82	0.847	3.32	232

2θ, scattering angle of (002) plane; FWHM, as calculated from the (002) plane; d_{002}, lattice spacing; SSA, specific surface area, as obtained from BET measurements.

surface populated by the chromophore units, such an increase in aggregation would still reflect modification of the surface.

3.2.3. TEM analysis

TEM analysis of selected samples such as GP (see Supporting Information (SI), Sec. 2), GP-Pnz, GP-Chr, GP-Fsc, and GP-Thio was performed. Fig. 3 shows TEM bright field phase contrast images and their corresponding Fast Fourier Transformation (FFT) power spectra for graphene nanoplatelets modified with phenazine, chromone, fluorescein and thionine molecules, respectively. In all cases the TEM images show a rather smooth surface (Fig. 3**a-d**), however the individual molecules cannot be resolved. Important findings emerge by analysing the FFTs of the images, which are equivalent to electron diffraction patterns. FFT for unmodified graphene samples displays a set of spots forming a hexagonal pattern characteristic for the graphene's honeycomb structure (SI, Sec. 2). In contrast, each FFT for modified graphene samples in Fig. 3**e-h** shows discrete sets of symmetrical spots, which belong to two separate types of patterns: hexagonal and quasi-rectangular. Since FFT power spectra represent reciprocal space, larger distances from the central spot correspond to smaller distances in real space. For the GP-Pnz sample there are two sets of spots, denoted by blue and white circles, that form two hexagonal patterns each characteristic of the graphene lattice viewed down the [0 0 1] direction and corresponding to the {1 0 0} type lattice spacing (Fig. 3**e**).

These two patterns are slightly rotated relative to each other corresponding to two different overlapping graphene nanoplatelets, which are randomly oriented on the TEM support film. The other two sets of spots, denoted by green and red circles, are much closer to the central spot and form two rectangular patterns. These additional spots were absent in the FFTs for the unmodified graphene (see SI, Sec. 2), suggesting that their presence in GP-Pnz FFT image (Fig. 3**e**) is associated with an ordered array of chromophores. Therefore, these spots correspond to two different domains of a phenazine layer attached to graphene surface. It is noted that the patterns for the phenazine domains are rotated relative to each other by the same angle as for the graphene patterns. Therefore, it is concluded that each graphene nanoplatelet is covered by a single well-ordered phenazine domain. Comparing the distances between individual spots from the phenazine domain and considering the graphene lattice parameter, the rectangular unit cell parameters of the phenazine layer are calculated to be 0.52 nm and 0.38 nm, in good agreement with a previous study of covalent modification of surface-supported graphene grown on cubic-SiC(0 0 1) by phenazine molecules [43]. The results therefore show that this modification method works well for the covalent attachment of phenazine molecules to graphene surfaces and the formation of ordered domains.

Similar results are observed for the FFT of the image of the GP-Chr sample (Fig. 3**f**), where two rectangular patterns (denoted by green and red circles respectively), rotated relative to each other by the same angle as for the graphene patterns, represent two different domains of the attached chromone layer. Therefore, it is concluded that each graphene nanoplatelet is covered by a single well-ordered Chr-domain. The unit cell parameters of the chromone layer are calculated to be 0.48 nm and 0.30 nm. The similarity of the FFT patterns obtained for GP-Pnz and GP-Chr samples is unsurprising since the molecules both attach to the graphene surface via C-C bonding of the fused aromatic ring system (Fig. 1, represented by a dashed line). Therefore, Pnz and Chr chromophores are both standing up on the surface [43] resulting in a comparable molecular layer pattern on graphene.

For the GP-Fsc and GP-Thio samples (Fig. 3**g,h**), there is one hexagonal pattern (spots denoted by white circles) that corresponds to a single graphene nanoplatelet. For both samples, one set of spots (denoted by red circles) forming an oblique unit cell, has been identified for the layer created by attached chromophore units. Hence, it is concluded that in each case graphene nanoplatelets are covered by a single well-ordered domain of the corresponding chromophore moieties. The calculated unit cell parameters are 0.63 nm and 0.32 nm for fluorescein layer and 0.91 nm and 0.44 nm for thionine layer.

Overall, the TEM/FFT results for the samples presented in Fig. 3 provide strong evidence that the modification methods described in this manuscript lead to formation of quite ordered domains of organic molecules bonded to the graphene surface. However, we note that disordered regions are also observed, presumably due to defects on the graphene surface and non-uniform nature of nanoplatelets. These disordered regions cannot be distinguished by TEM/FFT from non-modified graphene regions.

3.3. Dye removal study

Due to the presence of the functional groups, these materials can promote favourable electrostatic interactions and act as potential adsorbers for environmental contaminants such as dyes. To study the adsorption behaviour of graphene-based systems, the removal of methylene blue (MB), methyl orange (MO) and rhodamine B (RhB) in water was selected as a standard method [45–50]. Experiments were

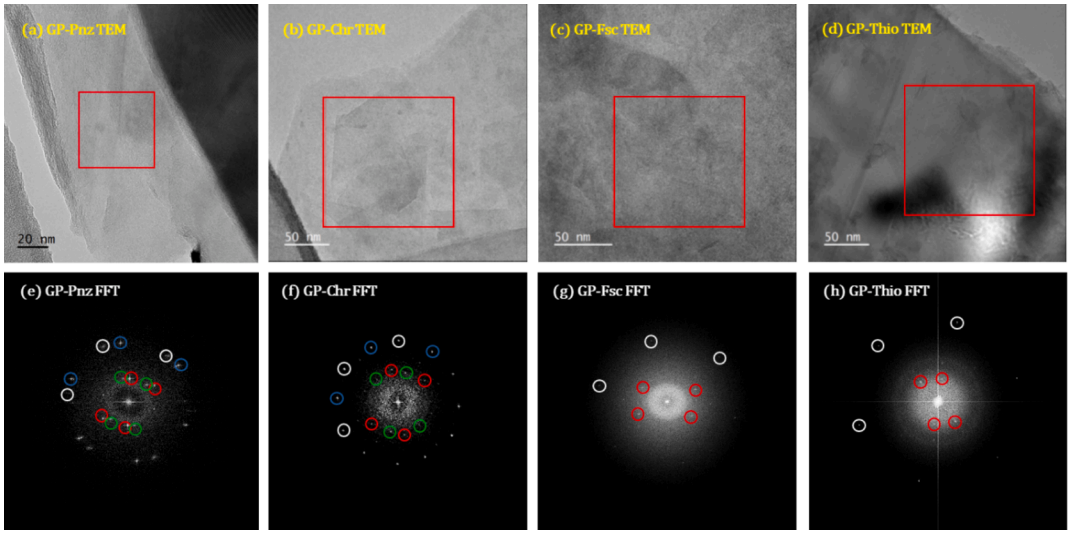

Fig. 3. TEM images and their Fast Fourier Transformations (FFTs) for the samples: (a) GP-Pnz TEM image; (b) GP-Chr TEM image; (c) GP-Fsc TEM image; (d) GP-Thio TEM image; (e) GP-Pnz FFT image; (f) GP-Chr FFT image; (g) GP-Fsc FFT image; (h) GP-Thio FFT image. The areas used to calculate FFT power spectra (e-g) are indicated by a red square in the corresponding TEM images (a-d).

conducted to identify the optimal loading range suitable for spectrophotometric monitoring. The calculated adsorption capacity (q) for the modified graphene materials (**SI Table S3**) varied between the samples and the optimal range was in a range of 0.0244–0.0476 g/L. Based on the accurate transmission window for the measurements, the concentration of 0.032 g/L was deemed to be optimal for comparative analysis of the removal of MB, MO and RhB. To determine the efficiency of dye removal, kinetic studies were carried out under pH 7 (22 °C) in the dark by recording UV–vis absorption spectra every 20 min during a 120 min experiment. The tested concentration of the GP materials was 0.0323 g/L and that of the dyes (adsorbents) were 3.0 mg/L for MB, 7.0 mg/L for MO and 4.6 mg/L for RhB. As MB and RhB are cationic dyes, whilst MO is a basic dye, it is expected that the trend in the adsorption capacity of the individual GP materials towards MB and RhB may be similar. The results of the adsorption studies and linear adjustment of pseudo-second order kinetic model are shown in Fig. 4 and **SI Sec. 3**. Pseudo-first order (PFO) (Eq. 1) and pseudo-second order (PSO) (Eq. 2) equations were used to assess behaviour of the composites and the data from non-linear fitting [51] is reported in Table 3 and Tables S4-S9. PSO Regression fit model has better correlation coefficient values (R^2) and the standard deviation error (SDE) for experimental (q_{exp}) and calculated ($q_{e\text{-}cal}$) values over PFO model.

Fig. 4 (right) shows the adsorption capacities of the modified GP materials for MO removal revealing relatively low values. The best results were achieved with GP-Acr (33.39 mg/g) and GP-Fsc (27.43 mg/g), which were closely followed by GP-Chr (25.04 mg/g). Other materials GP-AnOH, GP-Thio and GP-Pnz showed lower adsorption capacities plateauing at 20.27 mg/g, 16.69 mg/g and 13.12 mg/g, respectively. The structure of MO is not flat and therefore not favourable for efficient electrostatic interactions such as π-π stacking. Our results are in the middle of those adsorption capacities reported for GO (16.8 mg/g), carbon nano tubes (12.5–52.9 mg/g) and 3D graphene networks [52–55].

In contrast, MB adsorption was highest for GP-Fsc (49.6 mg/g), GP-Acr (47.92 mg/g) and GP-Thio (43.48 mg/g). This was followed by GP-Chr (38.31 mg/g), and then by GP-Pnz and GP-AnOH with a relatively similar adsorption capacities of 32.58 mg/g and 30.04 mg/g, respectively. The results for the first three materials are very encouraging; especially when the loading could be improved by optimising the concentration of the materials. They are in line with other examples from the literature for MB adsorption: zeolites (47.3, 22.0, and 5.6 mg/g), mesoporous activated carbon/zeolite composites (15.49, 47.95 mg/g), and activated carbon from biomass waste, chitosan-zeolites [56–59]. The lower adsorption capacity of GP-Chr is likely due to the only mild electrostatic interactions of the OH and C=O groups of the Chr-unit with N and S groups in MB, and a steric hindrance of the bulky Me groups. Although the surface area of GP-Pnz is smaller than that of GP-AnOH, its adsorption capacity is higher because of the preferential π-π stacking between Pnz-units and MB. The higher adsorption capacity of GP-Acr compared to others in the series is due to greater electrostatic attraction provided by π-π interactions.

Overall, the performance of the modified GP materials to remove RhB was better than that observed for MO and MB. A similar adsorption pattern to one observed for MB, was evident for GP-Fsc (63.35 mg/g) and GP-Acr (63.00 mg/g), which was closely followed by GP-AnOH (61.77 mg/g). Other materials also showed higher adsorption capacities with GP-Chr, GP-Thio and GP-Pnz being 58.19 mg/g, 45.08 mg/g and 33.15 mg/g, respectively.

Table 4 summarises the total amount of dye removed by the modified GP materials for all three model dyes. Similar to the adsorption capacity values, the removal of RhB was the most efficient (between 60–99 %), followed by MB (41–99 %), with the least efficient being MO (25–47 %). In this series, GP-Acr and GP-Fsc displayed the highest values for all three dyes, closely followed by GP-AnOH and GP-Chr with oxygen containing units, whilst GP-Thio and GP-Pnz were the least effective.

These results are influenced by multiple factors, with the mechanism of removal involving electrostatic interactions between the surface units and the dye molecules. The binding of molecules on surfaces is

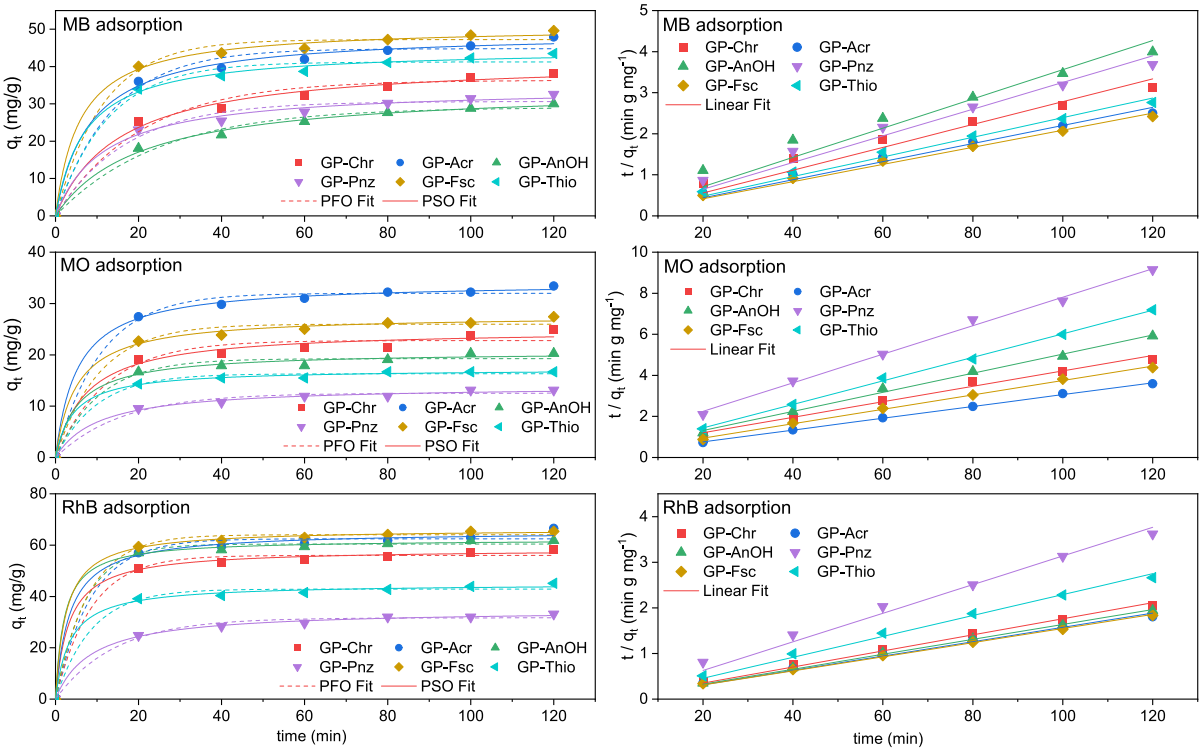

Fig. 4. (right) Summary of adsorption capabilities of MO, RhB and MB dyes for GP modified samples (0.0323 g/L) studied by spectrophotometric method monitoring absorbance decreases at 464 nm (MO), 664 nm (MB) and 553 nm (RhB) over 120 min; Pseudo-first order (PFO) and pseudo-second order (PSO) non-linear fitting curves. (left) Linear adjustment of pseudo-second order kinetic model.

Table 3
Pseudo-first order (PFO) and pseudo-second order (PSO) kinetic model parameters for the adsorption of MO, MB and RhB.

Model	Parameters	GP-Chr	GP-Acr	GP-AnOH	GP-Pnz	GP-Fsc	GP-Thio
PFO-MO	$q_{e\text{-}cal}$ ($mg\,g^{-1}$)	22.78	32.00	19.25	12.54	25.98	16.31
	k_1 (min^{-1})	0.081	0.092	0.094	0.063	0.096	0.101
	SDE	1.13	0.695	0.51	0.29	0.725	0.19
	R^2	0.966	0.993	0.982	0.981	0.988	0.991
PFO-MB	$q_{e\text{-}cal}$ ($mg\,g^{-1}$)	36.34	44.79	29.07	30.66	47.24	41.23
	k_1 (min^{-1})	0.049	0.073	0.040	0.058	0.088	0.080
	SDE	0.985	1.565	0.485	0.96	1.175	1.125
	R^2	0.974	0.981	0.982	0.973	0.989	0.986
PFO-RhB	$q_{e\text{-}cal}$ ($mg\,g^{-1}$)	56.00	62.48	60.44	31.68	64.06	42.87
	k_1 (min^{-1})	0.117	0.117	0.140	0.070	0.128	0.116
	SDE	1.095	2.03	0.665	0.735	0.645	1.105
	R^2	0.995	0.990	0.997	0.989	0.997	0.990
PSO-MO	$q_{e\text{-}cal}$ ($mg\,g^{-1}$)	24.94	34.15	20.65	14.01	27.72	17.25
	k_2 ($g\,mg^{-1}min^{-1}$)	0.0055	0.0056	0.0090	0.0069	0.0072	0.0134
	SDE	0.05	0.38	0.19	0.445	0.145	0.28
	R^2	0.982	0.999	0.992	0.993	0.996	0.997
PSO-MB	$q_{e\text{-}cal}$ ($mg\,g^{-1}$)	42.05	49.30	34.57	34.63	50.81	44.85
	k_2 ($g\,mg^{-1}min^{-1}$)	0.0015	0.0024	0.0014	0.0025	0.0034	0.0032
	SDE	1.87	0.69	2.265	1.025	0.61	0.685
	R^2	0.991	0.994	0.995	0.991	0.997	0.996
PSO-RhB	$q_{e\text{-}cal}$ ($mg\,g^{-1}$)	58.51	65.45	62.28	34.90	66.31	45.00
	k_2 ($g\,mg^{-1}min^{-1}$)	0.0053	0.0046	0.0077	0.0033	0.0060	0.0064
	SDE	0.16	0.545	0.255	0.875	0.48	0.04
	R^2	0.998	0.9951	0.999	0.997	0.999	0.996

Table 4
Summary of dye removal studies for the modified GP samples.

	MB removed, %	RhB removed, %	MO removed, %
GP-Chr	77	88	37
GP-Acr	94	99	47
GP-AnOH	85	86	32
GP-Pnz	41	60	25
GP-Fsc	99	90	41
GP-Thio	50	70	28

influenced by the dipole moments of the surface and the adsorbant, which can be permanent, induced or fluctuating [60]. It is likely that the orientation of the dye on the surface of GP is influenced by π-π stacking interactions; thus, a larger surface area should be a rate determining factor. The surface area of the modified GP materials decreased in the following order GP-Acr > GP-Fsc > GP-AnOH > GP-Thio > GP-Chr > GP-Pnz, but this alone cannot account for the activity observed. The low dye removal efficiencies of GP-Pnz and GP-Thio manifest from a lower surface area, but also from the presence of similar functional groups ($-NR_2$), which can cause electrostatic repulsion. The presence of a $-CO_2H$ group on GP-Fsc allows efficient binding of cationic MB and RhB leading to the formation of GP-Fsc*Dye salt, which can explain the excellent adsorption capacities. Although GP-AnOH and GP-Chr had surface areas almost half that of unmodified GP, they are able to bind the cationic dye through the presence of >C=O functional groups. GP-Acr had the largest surface area, and the presence of an imine (−N=) functional group allowed favourable dipole interactions with MB and RhB.

4. Conclusions

In summary, two-component hybrid graphene nanoplatelet systems have been fabricated and tested as potential materials for dye removal. Although a two-step procedure can be applied to a range of amines, it is limited by the stability of the corresponding diazonium salt and its tedious purification. To address these issues, an alternative one-pot synthetic methodology has been developed, which utilizes *in situ* generation of the diazonium salt, and is therefore applicable to a wide range of organic chromophores. The procedure is versatile and can be performed on a large scale, which offers an easy and cost-effective means of graphene modification. Detailed materials characterisation has been carried out to confirm the success of functionalization. All samples demonstrated tangible enhancements in optical properties, which are exclusively derived from the successful surface modification. XRD analysis of the modified samples showed a slight widening of the (0 0 2) graphitic peak relative to that of unmodified graphene, with no changes in the d_{002} spacing. Dramatic changes in BET and FT-IR data were due to chemical modifications on the surface and edges of the flakes. Although disordered regions are also observed, TEM analysis of selected samples GP-Chr, GP-Pnz, GP-Fsc and GP-Thio showed an ordered arrangement of the chromophore on the graphene platelet in good agreement with STM data previously reported for the GP-Pnz on Si(C) sample [43]. The hybrid materials were excellent absorbers for the removal of MO, MB and RhB dyes due to the diverse range of electrostatic interactions provided by organic units.

CRediT authorship contribution statement

Aminu Magaji: Writing – original draft, Validation, Methodology, Investigation, Formal analysis. **David P. Martin:** Validation, Methodology, Investigation, Conceptualization. **Li-Shang Lin:** Validation, Methodology, Formal analysis. **Sergey A. Krasnikov:** Writing – review & editing, Validation, Methodology, Formal analysis. **Alexander Kulak:** Methodology, Formal analysis. **Zabeada Aslam:** Validation, Methodology, Formal analysis. **Rik Drummond-Brydson:** Writing – review & editing, Validation, Supervision, Methodology. **Natalia N. Sergeeva:** Writing – review & editing, Writing – original draft, Validation, Supervision, Methodology, Conceptualization.

Declaration of competing interest

The authors declare that they have no known competing financial interests or personal relationships that could have appeared to influence the work reported in this paper.

Data availability

Data will be made available on request.

Acknowledgements

This research was partially supported by Clothworker's Innovation Fund. AM thanks Sule Lamido University Kafin-Hausa for the PhD studentship support and NS thanks Arts and Humanities Research Council (AH/X01021X/1) for partial support.

Appendix A. Supplementary data

Supplementary data to this article can be found online at https://doi.org/10.1016/j.jphotochem.2024.115884.

References

[1] A.C. Sophia, E.C. Lima, Ecotoxicol. Environ. Saf. 150 (2018) 1–17.
[2] S. Chowdhury, R. Balasubramanian, Adv. Colloid Interface Sci. 204 (2014) 35–56.
[3] S. Zhu, X. Huang, F. Ma, L. Wang, X. Duan, S. Wang, Environ. Sci. Tech. 52 (2018) 8649–8658.
[4] D. Saini, Gunture, J. Kaushik, R. Aggarwal, K.M. Tripathi, S.K. Sonkar, ACS Appl. Nano Mater. (2021).
[5] A. Mollar-Cuni, D. Ventura-Espinosa, S. Martín, H. García, J.A. Mata, ACS Catal. (2021) 14688–14693.
[6] H. Sun, C. Kwan, A. Suvorova, H.M. Ang, M.O. Tadé, S. Wang, Appl. Catal. B 154–155 (2014) 134–141.
[7] Y. Wang, X.C. Wang, M. Antonietti, Angew. Chem.-Int. Ed. 51 (2012) 68–89.
[8] N. Baig, Ihsanullah, M. Sajid, T.A. Saleh, J. Environ. Manage. 244 (2019) 370–382.
[9] Y. Zhu, S. Murali, W. Cai, X. Li, J.W. Suk, J.R. Potts, R.S. Ruoff, Adv. Mater. 22 (2010) 3906–3924.
[10] T. Kuila, S. Bose, A.K. Mishra, P. Khanra, N.H. Kim, J.H. Lee, Prog. Mater Sci. 57 (2012) 1061–1105.
[11] M. Hu, Z. Yao, X. Wang, Ind. Eng. Chem. Res. 56 (2017) 3477–3502.
[12] J. Zhang, Z. Xia, L. Dai, Sci. Adv. (2015) 1.
[13] S. Navalon, A. Dhakshinamoorthy, M. Alvaro, M. Antonietti, H. Garcia, Chem. Soc. Rev. (2017).
[14] X. Liu, L. Dai, Nat. Rev. Mater. 1 (2016) 16064.
[15] X. Li, J. Yu, S. Wageh, A.A. Al-Ghamdi, J. Xie, Small 12 (2016) 6640–6696.
[16] N. Zhang, Y. Zhang, Y.-J. Xu, Nanoscale 4 (2012) 5792–5813.
[17] H.-X. Wang, Q. Wang, K.-G. Zhou, H.-L. Zhang, Small 9 (2013) 1266–1283.
[18] F. Li, L. Zhang, J. Tong, Y. Liu, S. Xu, Y. Cao, S. Cao, Nano Energy 27 (2016) 320–329.
[19] H. Xiong, L.L. Jewell, N.J. Coville, ACS Catal. 5 (2015) 2640–2658.
[20] J. Albero, D. Mateo, H. García, Molecules 24 (2019) 906.
[21] A.A. Ismail, D.W. Bahnemann, Sol. Energy Mater. Sol. Cells 128 (2014) 85–101.
[22] D. Salinas-Torres, M. Navlani-García, K. Mori, Y. Kuwahara, H. Yamashita, Appl. Catal. A 571 (2019) 25–41.
[23] A. Quintanilla, J. Carbajo, J.A. Casas, P. Miranzo, M.I. Osendi, M. Belmonte, Catal. Today 356 (2020) 197–204.
[24] F. Opoku, K.K. Govender, C.G.C.E. van Sittert, P.P. Govender, Adv. Sustain. Syst. 1 (2017) 1700006.
[25] Y. Lin, Y. Tian, H. Sun, T. Hagio, Chemosphere 270 (2021) 129420.
[26] M. Wang, L. Cai, Y. Wang, F. Zhou, K. Xu, X. Tao, Y. Chai, J. Am. Chem. Soc. 139 (2017) 4144–4151.
[27] K. He, G. Chen, G. Zeng, A. Chen, Z. Huang, J. Shi, T. Huang, M. Peng, L. Hu, Appl Catal B 228 (2018) 19–28.
[28] Q. Xiang, J. Yu, M. Jaroniec, Chem. Soc. Rev. 41 (2012) 782–796.
[29] J. Yu, J. Jin, B. Cheng, M. Jaroniec, J. Mater. Chem. A 2 (2014) 3407–3416.
[30] P.-Q. Wang, Y. Bai, P.-Y. Luo, J.-Y. Liu, Catal. Commun. 38 (2013) 82–85.
[31] C. Lee, X. Wei, W. Kysar Jeffrey, J. Hone, Science 321 (2008) 385–388.
[32] S. Chen, Q. Wu, C. Mishra, J. Kang, H. Zhang, K. Cho, W. Cai, A.A. Balandin, R. S. Ruoff, Nat. Mater. 11 (2012) 203–207.
[33] K.S. Novoselov, V.I. Fal'ko, L. Colombo, P.R. Gellert, M.G. Schwab, K. Kim, Nature 490 (2012) 192–200.
[34] Y. Zongyou, Z. Jixin, H. Qiyuan, C. Xiehong, T. Chaoliang, C. Hongyu, Y. Qingyu, H. Zhang, Adv. Energy Mater. 4 (2014) 1300574.
[35] J. Zhang, L. Dai, ACS Catal. 5 (2015) 7244–7253.
[36] V. Georgakilas, M. Otyepka, A.B. Bourlinos, V. Chandra, N. Kim, K.C. Kemp, P. Hobza, R. Zboril, K.S. Kim, Chem. Rev. 112 (2012) 6156–6214.
[37] J. Park, M. Yan, Acc. Chem. Res. 46 (2013) 181–189.
[38] A. Hirsch, J.M. Englert, F. Hauke, Acc. Chem. Res. 46 (2013) 87–96.
[39] J.M. Englert, C. Dotzer, G. Yang, M. Schmid, C. Papp, J.M. Gottfried, H.-P. Steinrück, E. Spiecker, F. Hauke, A. Hirsch, Nat. Chem. 3 (2011) 279–286.
[40] E. Bekyarova, M.E. Itkis, P. Ramesh, C. Berger, M. Sprinkle, W.A. de Heer, R. C. Haddon, J. Am. Chem. Soc. 131 (2009) 1336–1337.
[41] K.S. Mali, J. Greenwood, J. Adisoejoso, R. Phillipson, S. De Feyter, Nanoscale 7 (2015) 1566–1585.
[42] D.P. Martin, A. Tariq, B.D.O. Richards, G. Jose, S.A. Krasnikov, A. Kulak, N. N. Sergeeva, Chem. Commun. 53 (2017) 10715–10718.
[43] N.N. Sergeeva, A.N. Chaika, B. Walls, B.E. Murphy, K. Walshe, D.P. Martin, B.D. O. Richards, G. Jose, K. Fleischer, V.Y. Aristov, O.V. Molodtsova, I.V. Shvets, S. A. Krasnikov, Nanotechnology 29 (2018) 275705.
[44] H.-M. Ju, S.H. Huh, S.-H. Choi, H.-L. Lee, Mater. Lett. 64 (2010) 357–360.
[45] T. Soltani, M.H. Entezari, J. Mol. Catal. A Chem. 377 (2013) 197–203.
[46] R.S. Dariani, A. Esmaeili, A. Mortezaali, S. Dehghanpour, Optik 127 (2016) 7143–7154.
[47] S.K. Tammina, B.K. Mandal, N.K. Kadiyala, Environ. Nanotechnol. Monit. Manage. 10 (2018) 339–350.
[48] S. Thakur, P. Das, S.K. Mandal, ACS Appl. Nano Mater. 3 (2020) 5645–5655.
[49] H. Maleki, V. Bertola, ACS Appl. Nano Mater. 2 (2019) 7237–7244.
[50] M.T. Vallejo-Macías, C.L. Recio-Colmenares, J.B. Pelayo-Vázquez, S. Gómez-Salazar, F. Carvajal-Ramos, J.F. Soltero-Martínez, M. Vázquez-Lepe, J.D. Mota-Morales, M.G. Pérez-García, ACS Appl. Nano Mater. 3 (2020) 5794–5806.
[51] S.R. Mishra, R. Verma, V. Gadore, M. Ahmaruzzaman, Biomass Convers. Biorefin. (2023).
[52] D. Robati, B. Mirza, M. Rajabi, O. Moradi, I. Tyagi, S. Agarwal, V.K. Gupta, Chem. Eng. J. 284 (2016) 687–697.
[53] H.Y. Zhu, R. Jiang, L. Xiao, G.M. Zeng, Bioresour. Technol. 101 (2010) 5063–5069.
[54] C. Karaman, O. Karaman, P.-L. Show, Y. Orooji, H. Karimi-Maleh, Environ. Res. 207 (2022) 112156.
[55] C. Hu, D. Grant, X. Hou, F. Xu, Mater. Today Proc. 34 (2021) 184–193.
[56] F. Mohamed, M. Shaban, S.K. Zaki, M.S. Abd-Elsamie, R. Sayed, M. Zayed, N. Khalid, S. Saad, S. Omar, A.M. Ahmed, A. Gerges, H.R.A. El-Mageed, N. K. Soliman, Sci. Rep. 12 (2022) 18031.
[57] Z. Shui, L. Yao, X. Pu, L. Yang, W. Jiang, X. Jiang, Ind. Eng. Chem. Res. 59 (2020) 14616–14624.
[58] W.A. Khanday, F. Marrakchi, M. Asif, B.H. Hameed, J. Taiwan Inst. Chem. Eng. 70 (2017) 32–41.
[59] K.D. Lokhande, D.A. Pethsangave, D.K. Kulal, S. Some, ChemistrySelect 5 (2020) 8062–8073.
[60] E. Voloshina, D. Usvyat, M. Schütz, Y. Dedkov, B. Paulus, PCCP 13 (2011) 12041–12047.